

Reliability and Feasibility of Low-Field-Strength Fetal MRI at 0.55 T during Pregnancy


Jordina Aviles Verdera, MSc • Lisa Story, PhD, MD • Megan Hall, MD • Tom Finck, MD • Alexia Egloff, MD • Paul T. Seed, PhD • Shaihan J. Malik, PhD • Mary A. Rutherford, MD • Joseph V. Hajnal, PhD • Raphaël Tomi-Tricot, PhD • Jana Hutter, PhD

From the Centre for the Developing Brain, School of Biomedical Engineering & Imaging Sciences, King's College London, 1st Floor South Wing, St Thomas' Hospital, Westminster Bridge Road SE1 7EH London, United Kingdom (J.A.V., L.S., M.H., P.T.S., S.J.M., M.A.R., J.V.H., J.H.); Centre for Medical Biomedical Engineering Department, School of Biomedical Engineering and Imaging Sciences, King's College London, London, UK (J.A.V., L.S., A.E., S.J.M., M.A.R., J.V.H., J.H.); Women's Health, GSTT, London, UK (L.S., M.H., T.F., P.T.S.); Technical University Munich, Munich, Germany (T.F.); MR Research Collaborations, Siemens Healthcare Limited, Camberley, UK (R.T.T.); and Radiological Institute, University Hospital Erlangen, Erlangen, Germany (J.H.). Received November 30, 2022; revision requested January 25, 2023; final revision received August 20; accepted September 6. **Address correspondence to** J.H. (email: jana.hutter@kcl.ac.uk).

Supported by a Wellcome Trust Collaboration in Science grant (WT201526/Z/16/Z); J.H. supported by a United Kingdom Research and Innovation Future Leaders Fellowship (MR/T018119/1); L.S. supported by an NIHR Advanced Fellowship (NIHR3016640) and by core funding from the Wellcome/Engineering and Physical Sciences Research Council Centre for Medical Engineering (WT203148/Z/16/Z).

Conflicts of interest are listed at the end of this article.

See also the editorial by Gowland in this issue.

Radiology 2023; 309(1):e223050 • <https://doi.org/10.1148/radiol.223050> • Content codes:  

Background: The benefits of using low-field-strength fetal MRI to evaluate antenatal development include reduced image artifacts, increased comfort, larger bore size, and potentially reduced costs, but studies about fetal low-field-strength MRI are lacking.

Purpose: To evaluate the reliability and feasibility of low-field-strength fetal MRI to assess anatomic and functional measures in pregnant participants using a commercially available 0.55-T MRI scanner and a comprehensive 20-minute protocol.

Materials and Methods: This prospective study was performed at a large teaching hospital (St Thomas' Hospital; London, England) from May to November 2022 in healthy pregnant participants and participants with pregnancy-related abnormalities using a commercially available 0.55-T MRI scanner. A 20-minute protocol was acquired including anatomic T2-weighted fast-spin-echo, quantitative T2*, and diffusion sequences. Key measures like biparietal diameter, transcerebellar diameter, lung volume, and cervical length were evaluated by two radiologists and an MRI-experienced obstetrician. Functional organ-specific mean values were given. Comparison was performed with existing published values and higher-field MRI using linear regression, interobserver correlation, and Bland-Altman plots.

Results: A total of 79 fetal MRI examinations were performed (mean gestational age, 29.4 weeks \pm 5.5 [SD] [age range, 17.6–39.3 weeks]; maternal age, 34.4 years \pm 5.3 [age range, 18.4–45.5 years]) in 47 healthy pregnant participants (control participants) and in 32 participants with pregnancy-related abnormalities. The key anatomic two-dimensional measures for the 47 healthy participants agreed with large cross-sectional 1.5-T and 3-T control studies. The interobserver correlations for the biparietal diameter in the first 40 consecutive scans were 0.96 (95% CI: 0.7, 0.99; $P = .002$) for abnormalities and 0.93 (95% CI: 0.86, 0.97; $P < .001$) for control participants. Functional features, including placental and brain T2* and placental apparent diffusion coefficient values, strongly correlated with gestational age (mean placental T2* in the control participants: 5.2 msec of decay per week; $R^2 = 0.66$; mean T2* at 30 weeks, 176.6 msec; $P < .001$).

Conclusion: The 20-minute low-field-strength fetal MRI examination protocol was capable of producing reliable structural and functional measures of the fetus and placenta in pregnancy.

Clinical trial registration no. REC 21/LO/0742

© RSNA, 2023

Supplemental material is available for this article.

Fetal MRI is increasingly valuable for a variety of clinical conditions because of recent advances in acquisition and analysis in diagnosis of subtle neurology (1), morphologic cues aiding prediction of spina bifida outcomes, elucidation of complex congenital heart disease allowing for postnatal surgical planning (2), and morphologic changes before preterm birth (3,4), all of which enhance antenatal counseling. Functional imaging provides detailed insights: diffusion-weighted MRI depicts vascular pathologic abnormalities (5–9), perfusion helps to detect white matter anomalies, and T2* relaxometry (10,11) has depicted placental abnormalities

(12–14). Finally, dynamic techniques provide insight into fetal mobility.

Fetal MRI, which is usually performed at 1.5 T but increasingly is performed at 3 T to use the higher signal-to-noise ratio, is subject to challenges. These challenges are related to an increase in magnetic field: susceptibility-induced B_0 inhomogeneities because they originate between maternal bowel and fetal tissue result in geometric distortion artifacts (Fig 1A, 1B) and increase with field strength. These limit the use of mainly functional data unless dedicated image-based correction (15) is applied. B_1 inhomogeneities also increase with field strength and are amplified

Abbreviations

ADC = apparent diffusion coefficient, BMI = body mass index

Summary

A 20-minute low-field-strength 0.55-T fetal MRI examination performed with a commercial scanner allowed for robust assessment of fetal growth and placental function while increasing patient comfort and decreasing the need for specialist centers.

Key Results

- In a prospective study of 79 fetal MRI examinations, a 20-minute 0.55-T protocol not requiring B_0 or B_1 artifact correction allowed full anatomic assessment in 20 of 21 clinically referred participants with pregnancy-related pathologic abnormalities.
- Biparietal diameter, a key clinical anatomic measure, had an interobserver correlation of 0.93 ($P < .002$) for healthy control participants and 0.96 ($P < .001$) for pathologic abnormalities, in line with published large cross-sectional 1.5-T and 3-T studies.
- In control participants, functional mean $T2^*$ values of brain (281.5 msec at 30 weeks gestational age) and placenta (176.6 msec at 30 weeks gestational age) correlated with gestational age ($R^2 = 0.54$ and 0.66 , respectively; both $P < .001$).

at fetal MRI because of the large conducting volume of the amniotic fluid (Fig 1B).

The longer $T2^*$ at low field strength has the benefit of more efficient sampling of the signal; and the shorter $T1$ decreases repetition time without risking insufficient signal recovery (15). Reliance on superconducting magnets results in typical bore sizes of 60–70 cm for 1.5-T and 3-T MRI scanners, which excludes many pregnant individuals (16) and reduces comfort. Finally, regardless of magnet strength, unpredictable motion patterns and the resulting reliance on single-shot echo-planar imaging techniques render fetal examinations more susceptible to B_0 artifacts. Exploiting lower field MRI systems could mitigate some of these challenges but may introduce reduced signal-to-noise. The lower field strength allows increasing the bore size, which gives more pregnant individuals access to fetal MRI. Contemporary low-field-strength systems include recent pulse sequence developments and the ability to integrate and optimize custom-made sequences for faster scan times. Studies of fetal MRI with a commercially available 0.55-T scanner are lacking.

We hypothesize that a 20-minute fetal MRI protocol on a commercially available 0.55-T scanner allows diagnostic image quality for both anatomic and functional imaging. The purpose of this study was to evaluate the reliability and feasibility of such a low-field-strength fetal MRI protocol.

Materials and Methods

One of the authors (R.T.T.) is an employee of Siemens Healthineers. This author had no control of the data or information submitted for publications. Data and all analysis code are available for interested researchers (<https://github.com/JordinaAviles>).

Participants

In a prospective trial, pregnant participants were recruited to an institutional review board–approved study (REC 21/LO/0742) and provided written informed consent. The study

was performed between May and November 2022 at a large teaching hospital (St Thomas' Hospital, London, England). Exclusion criteria included age younger than 16 years and age older than 55 years, contraindications for MRI, and body weight greater than 220 kg (limitations related to the evacuation procedure). Participants with a body mass index (BMI) (in kilograms of body weight per meters of height squared) greater than 30 were considered to have a high body mass index.

Data sets were acquired by using a clinical 80-cm bore (Fig 1A) 0.55-T system (Magnetom Free.Max; Siemens Healthineers) with a blanket-like BioMatrix Contour-L six-element coil and a fixed nine-element spine coil (Siemens Healthineers).

$T2^*$ data from a study performed at the same institution with matched criteria acquired at 1.5 T (56 healthy control participants) and 3 T (104 healthy control participants) were included to offer comparative evaluation (Table S1).

Participant Preparation

Pregnant participants were scanned in a headfirst supine position or a slight left tilt with head, back, and leg cushioning as required. Continuous heart rate and intermittent blood pressure were monitored together with frequent verbal interaction to identify any vasovagal episode. Specific absorption rate was limited to normal mode. Nine pregnant participants who underwent 0.55-T and 1.5- or 3-T fetal MRI were asked to assess comfort on a scale from 1 (not comfortable) to 5 (very comfortable).

Core Low-Field-Strength MRI Protocol

The protocol was designed to allow completed radiologic assessment of anatomic structures as well as quantitative assessment of the most common functional contrasts. All parameters are given in detail in Table 1.

The protocol included a structural $T2$ -weighted single-shot turbo spin-echo clinical sequence optimized for fetal contrast enhancement and acquired in a total of six directions, three covering the entire uterus and three focused on the fetal brain. A field of view of 400×400 mm² was chosen to allow for robust imaging, even in participants with BMIs greater than 40, and the voxel size was increased compared with the 1.5-T or 3-T protocols.

In line with other commonly used fetal protocols, $T2^*$ mapping and diffusion MRI were chosen and performed sequentially without repositioning. Importantly, and different than conventional protocols at higher field strength, no calibration scans were included and no efforts beyond automatic vendor-supplied shimming were performed, reducing examination time compared with similar higher field setups.

A gradient-echo single-shot echo-planar imaging sequence was used for $T2^*$ relaxometry. Diffusion MRI data were acquired with a single-shot diffusion-weighted spin-echo sequence with seven b values between 0 and 1000 sec/mm². Finally, dynamic cine scans were acquired to image fetal motion.

Analysis and Quantitative Measures

The analysis of all acquired data sets followed standard processes. All anatomic stacks were used to assist radiologic brain reports. Key brain features including the biparietal diameter

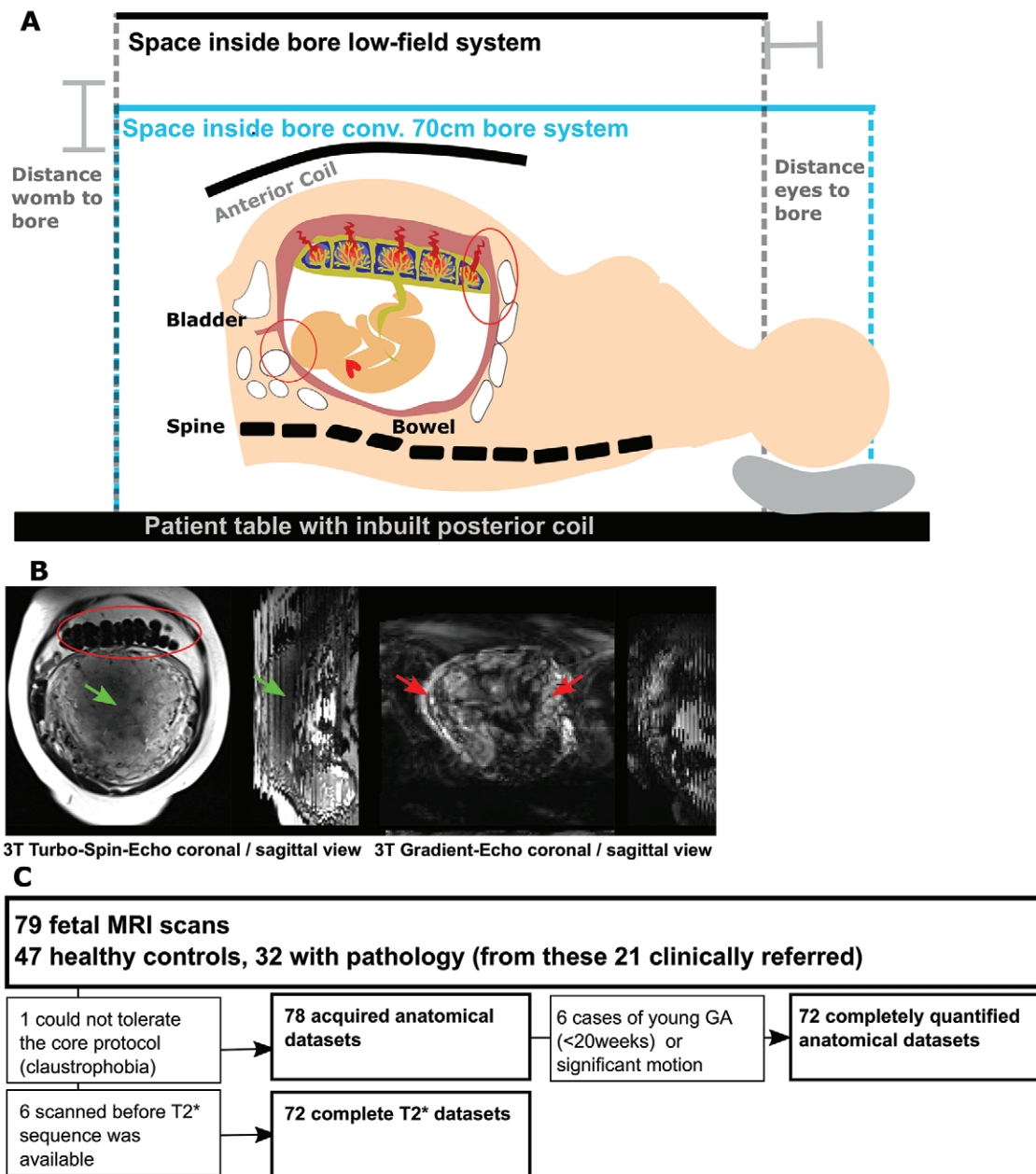


Figure 1: (A) Schemata of the patient preparation including the fetal 0.55-T MRI bore, MRI table, posterior and anterior coils (in black), and maternal and fetal structures of interest for the imaging process, most notably bladder, spine, and bowel. The uterus-to-bore and eyes-to-bore distances are shown. Red circles show areas of obvious air-tissue interfaces between the transverse bowel and fundal parts of the placenta and between the fetal head in cephalic position and the rectum. (B) Exemplary 3-T data show T2-weighted fast-spin-echo and gradient-echo fetal MRI data on coronal and sagittal views. Images show B_1 inhomogeneities (green arrows) and distortion effects from B_0 inhomogeneities (red arrows). (C) Flow diagram of included participants. conv. = conventional, GA = gestational age.

and transcerebellar diameter were obtained following previously described protocols and normative curves (17) by two radiologists (M.A.R., with 20 years of experience in fetal radiology, or A.E., with 10 years of experience in neuroradiology). The first 40 MRI examinations (among these 40 cases were six with abnormalities) were independently double-read (M.A.R. and T.F., with 8 years of experience in radiology), the interobserver variability was reported, and disagreements were resolved by consensus. The cervical length (measured

from internal to external os) and the lung volume were assessed by a consultant obstetrician (L.S., with 8 years of experience in fetal MRI).

The anatomic measurements were then compared with normal curves from the literature obtained at 1.5-T and 3-T MRI or US, including the Rypens formula for lung volume double-read biparietal diameters and transcerebellar diameters to evaluate reliability and robustness (18–20). Finally, the image quality, percentage of sections with artifacts, and the ability to

Table 1: Scan Parameters for All Sequences

Parameter	Anatomic Imaging	Diffusion MRI	T2* Relaxometry	Dynamic Cine
Sequence	2D single-shot fast spin echo	Diffusion-weighted, 2D, single-shot, spin-echo, echo-planar imaging	Single-shot, multiecho, gradient-echo, echo-planar imaging	2D single-shot fast spin echo
Coverage and orientation	Six stacks, three focusing on the whole uterus, three planned in radiologic fetal brain planes	Coronal to the mother	Coronal to the mother, whole uterus	One single thick-section planned to the fetal body
Field of view (mm ²)	450 × 450	400 × 400	400 × 400	450 × 450
No. of sections	20–55	36	50	1
Resolution (mm ³)	1.5 × 1.5 × 4.5	3 × 3 × 3	4 × 4 × 4	2.8 × 2.8 × 10
Acceleration				
Partial Fourier	4/8	6/8	8/8	5/8
In-plane acceleration	2	2
TR (msec)	2500	7200	19,170	4000*
TE (msec)	106	129	46, 120, 194, 268, 342	103 [†]
<i>b</i> values (sec/mm ²)	NA	0, 10, 50, 80, 200, 400, 600, 1000	NA	NA
Acquisition time (min)	12 (2:57 × 3 + 1:05 × 3)	2:46	1:06	2:02
Obtained parameters	Transcerebellar diameters, biparietal diameters, lung volume, cervical length	Mean apparent diffusivity coefficient	Mean T2* placenta, volume placenta, mean T2* brain, volume brain	Dynamic information on motion

Note.—Data in parentheses are equations used to find the acquisition time for anatomic imaging. NA = not applicable, TE = echo time, TR = repetition time, 2D = two-dimensional.

* To allow sufficient signal recovery.

[†] Thirty dynamics.

perform a full clinical radiologic report were assessed as qualitative scores for all clinically referred participants.

The placenta and brain were manually segmented on T2* and diffusion data by an experienced fetal MRI physicist (J.H., with 8 years of experience), excluding images visually corrupted by crude motion or subclinical contractions. Quantitative modeling resulted in mean T2* time in milliseconds; diffusivity, known as *D*, in millimeters per seconds squared for the simple apparent diffusion coefficient (ADC) model; perfusion fraction, known as *f*, in percentage; and diffusivity, known as *D*, in millimeters per second squared, and pseudodiffusivity, known as *D*^{*}, in millimeters per second squared, for the more complex model. See Appendix S1 for additional analysis details.

Statistical Analysis

The intraclass correlation for the biparietal diameter and the transcerebellar diameter were calculated using a one-way analysis of variance fixed-effects model to evaluate the reliability of ratings by comparing the variability of different ratings in the same participant to the total variation across all ratings and all participants using statistical software (Python package pingouin 0.5.2; Python Software Foundation).

Linear regression analysis was performed for the functional values (mean T2* and volume of the placenta and brain, ADC, *D*^{*}, and perfusion fraction of the placenta)

using statistical software (Python package scipy 1.9.2; Python Software Foundation).

Bland-Altman plots and analysis were performed to evaluate consistency between biparietal diameters and transcerebellar diameters as well as repeated T2* quantities in Python.

P < .005 was used to indicate statistical significance. One author (P.T.S.) is a senior lecturer in statistics and was involved in verifying the statistical tests used.

Results

Participant Characteristics

Seventy-nine examinations were included in this study (Table 2; Figs 1C, S1). The core protocol was well tolerated in all participants except one; the examination was stopped prematurely because of maternal anxiety in this participant. Thereby, 47 pregnant participants fit the category of low-risk control pregnancies, with no clinical indication for MRI, and no diagnosis of pre-eclampsia, fetal growth restriction, diabetes, neurologic abnormalities, or other clinically significant complications. There were 32 participants with pregnancy-related pathologic abnormalities; their details are provided in Table 2. Among these participants, 21 were clinically referred because of pre-existing claustrophobia, BMI above 30, or lack of availability of a higher field scanner. Of the 32 participants, 12 scans

Table 2: Participant Characteristics

Parameter	Value
Mean gestational age at scan (wk)	29.37 ± 5.46 (17.6–39.28)
No. of women	79
Maternal age (y)	34.37 ± 5.28 (18.44–45.5)
Mean maternal body mass index	27.29 ± 5.99 (18.4–49.82)
No. of singleton pregnancies	79
No. of healthy pregnancies	47
No. of neurologic abnormalities	12
Midline cyst	1*
Scalp tumor	1*
Ventriculomegaly	6*
Mega/dilated cisterna magna	2*
Head smaller than 4th centile	1*
Large head/prominent lateral ventricles	1*
No. of placental-related disease and body anomalies	18
Partial molar pregnancy	1*
Pre-eclampsia and placental infarct	1
Fetal growth restriction	1
Prolonged preterm rupture of the membranes and funnel	5
Cytomegalovirus	2*
Trisomy 21	1*
Placental insufficiency	1
Lupus, cholestasis	1
Cystic kidney	1*
Calcifications thorax	1*
Amniotic band	1*
Multiple pathologic abnormalities	1*
Hypoplastic left heart syndrome	1*
Diabetes type 1	2

Note.—Mean data are ± SDs; data in parentheses are ranges. These were referred by standard clinical referral pathways. A total of 19 pregnant participants had a body mass index (in kilograms of body weight per meters of height squared) greater than 30.

* These 21 participants were referred clinically and thus required a full clinical report.

showed a clinical neurologic indication; 18 showed a placental pathology, fetal body anomaly, or infection indication; and two scans were acquired in pregnant participants with type 1 diabetes mellitus. Details are provided in Table 3.

Twenty-one participants were referred clinically and thus required a full clinical report (Table 2). From the entire cohort, a total of 19 pregnant participants had a BMI greater than 30.

Anatomic Data and Radiologic Evaluation

Whole uterus coronal views are depicted for different gestational age ranges (Fig 2A) together with an enlarged view of the fetal brain on three radiologic planes (Fig 2B) and in the lungs

(Fig 2C). The first 40 participants are also depicted in Figure S2. The radiographers were able to obtain the prescribed imaging planes in similar quality to higher field protocols. Fetal lung volumes were obtained for all participants, cervical length was measured in all but four participants (two participants with preterm prelabor rupture of the membranes), biparietal diameters could not be measured on three scans (two scans obtained at <20 weeks), and transcerebellar diameter measurements could not be measured on six scans (all scans obtained at <25 weeks). Figure 3 shows these measurements against gestational age for the entire sample together with the regression results for the control participants, fifth and 95th centile curves from normative literature (19–22). The interobserver correlations for the biparietal diameter between both radiologists were as follows for the control cohort, the cohort with abnormalities: 0.93 (95% CI: 0.86, 0.97; $P < .001$) and 0.96 (95% CI: 0.7, 0.99; $P = .002$), respectively. The interobserver correlations for the transcerebellar diameter were as follows for the control cohort and the cohort with pathologic abnormalities: 0.95 (95% CI: 0.88, 0.98; $P < .001$) and 0.95 (95% CI: 0.64, 0.99; $P = .003$), respectively. The radiologic assessment showed a mean data quality score of 2.6 (of 3). A full report was possible in 20 of 21 scans, and 15 of 21 scans had less than 10% of sections with artifacts (Fig 4A–4C, Table S2).

The survey regarding participant comfort resulted in a mean value of 4.3 ± 0.7 (from 1, not comfortable, to 5, very comfortable) for the low-field-strength scanner (all examinations performed at 0.55 T with an 80-cm bore) compared with 2.9 ± 0.8 for the 1.5-T and 3-T scanners (Fig 4D).

Observing Clinical Findings and Incidental Findings

Figure 4E and 4F show seven concrete clinical findings and incidental findings (neurologic deviations and uterine findings), and placental and ovarian findings were compared with 3-T data where available. Finally, Movies 1–3 depict limb and hand motion and cardiac activity on the dynamic cine videos.

Functional Data

Derived quantitative maps displayed a pattern of high T2* in the lobule centers with reduced T2* in the placental septa and toward the periphery of the placenta (Figs 5, S3). Similarly, the brain T2* map demonstrated reduced T2* toward the basal ganglia and increased T2* toward the cortex. The diffusion data (Fig 5) with increasing diffusion weighting show the expected decay in signal and changing contrast enhancement. The final placental map shows a pattern of increased ADC in the lobule centers with reduced ADC in the septa. Similarly, the brain map shows the expected pattern across white matter, gray matter, and cortex.

Mean T2* values together with volumes from large in-house studies to enable cross-field strength comparisons are shown in Figure 6A–6D. The obtained quantitative regression results for the T2* measurements on all three cohorts at three field strengths are depicted in Table 3. Placental volume (Fig 6A) showed a positive correlation with gestational age (25.9 mL of growth per week; 95% CI: 18.7, 33.0; $R^2 = 0.64$; $P < .001$), well in the range of results from 1.5-T and 3-T scanners (1.5-T and 3-T scanners,

Table 3: Rates of Change in Standard Functional Parameters with Gestational Age for the Three Control Cohorts Scanned at Different MRI Field Strengths

Parameter	0.55-T Field Strength (n = 47)			1.5-T Field Strength (n = 56)			3-T Field Strength (n = 104)		
	Value	R ² Value	P Value	Value	R ² Value	P Value	Value	R ² Value	P Value
Gestational age (wk)*	29.0 ± 6.0 (17.6–39.3)	30.0 ± 5.5 (18.6–38.6)	30.2 ± 4.7 (15.7–38.6)
Change in T2* placenta volume per week (mL)	25.9 (18.7, 33.0)	0.64	<.001	21.6 (14.2, 29.1)	0.38	<.001	17.4 (10.8, 24.0)	0.21	<.001
Total volume at 30 weeks	447.5	406.8	387.91
Change in T2* placenta mean per week (msec)	-5.2 (-6.6, -3.9)	0.66	<.001	-4.7 (-5.9, -3.5)	0.52	<.001	-2.9 (-3.4, -2.5)	0.59	<.001
At 30 weeks	176.6	112.4	56.4
Change in T2* brain volume per week (mL)	20.3 (17.9, 22.6)	0.92	<.001	16.9 (14.8, 19.0)	0.84	<.001	20.9 (17.9, 23.9)	0.81	<.001
Total volume at 30 weeks	230.6	166.2	196.6
Change in T2* brain mean per week (msec)	-6.8 (-9.2, -4.3)	0.54	<.001	-4.7 (-6.1, -3.3)	0.50	<.001	-7.5 (-9.3, -5.6)	0.60	.001
At 30 weeks	281.5	237.12	164.02

Note.—Unless otherwise indicated, data in parentheses are 95% CIs. Only control pregnancies not diagnosed with placental, neurologic disease, and diabetes type 1. All P values indicated statistical significance.

* Data in parentheses are ranges of gestational weeks.

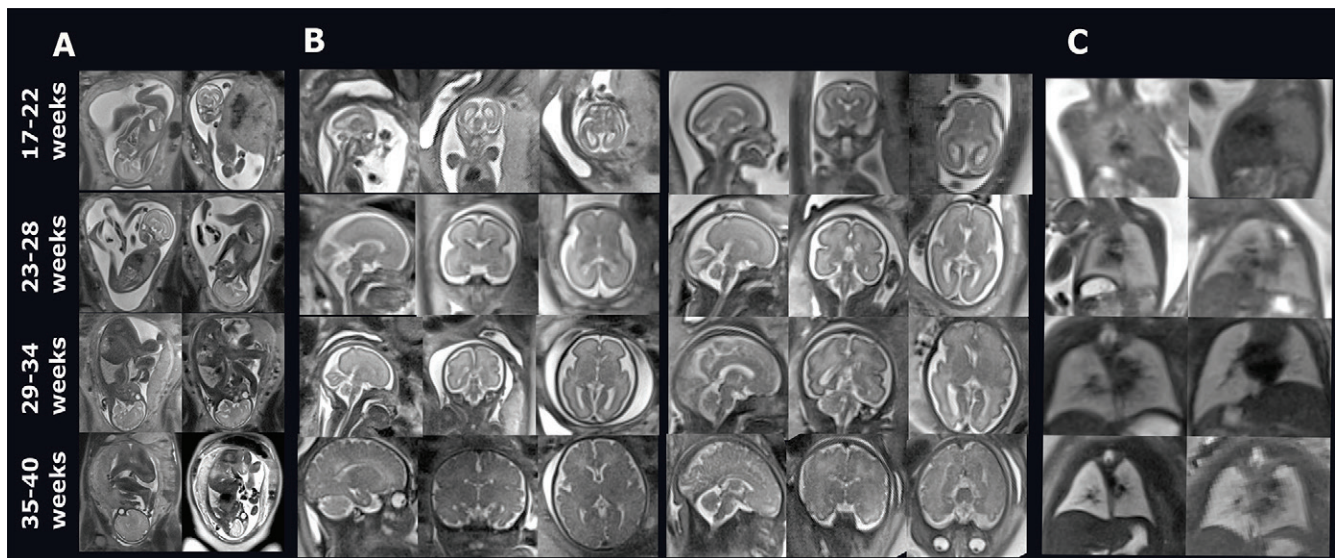


Figure 2: Images show fetal T2-weighted fast-spin-echo 0.55-T MRI scans at various gestational ages. (A) Miduterine coronal anatomic views from eight representative healthy pregnant participants (scans in control participants); (B) planned brain views in sagittal, coronal, and axial orientation from eight representative healthy pregnant participants (scans in control participants); and (C) lung views from eight representative healthy pregnant participants (scans in control participants). The scans are shown in four gestational age ranges.

respectively: 21.6 mL of growth per week [95% CI: 14.2, 29.1] and 17.4 mL [95% CI: 10.8, 24.0]). A clear negative correlation between mean placental T2* and gestational age (Fig 6B) was observed (5.2 msec of decay per week; R² = 0.66; P < .001), with

mean T2* reaching 176.6 at 30 weeks gestational age, above the respective values at 1.5 T and 3 T, as expected. Brain volumes (Fig 6C) were strongly correlated with gestational age (20.3 mL of growth per week; 95% CI: 17.9, 2.6; R² = 0.92; P < .001) and

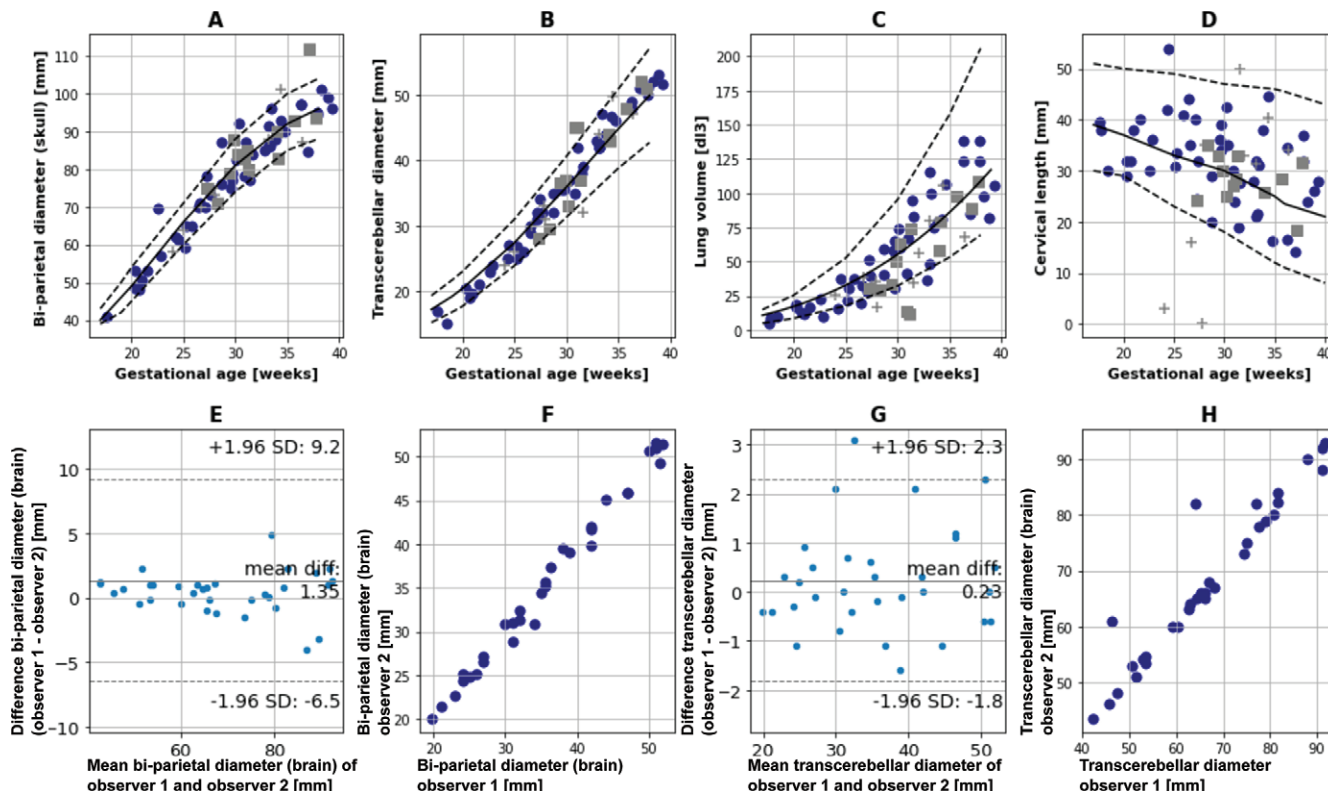


Figure 3: Plots show anatomic measures obtained at anatomic two-dimensional fast-spin-echo fetal 0.55-T MRI in the healthy pregnant participant cohort at different gestational ages. **(A)** Biparietal diameter of the brain (skull), **(B)** transcerebellar diameter, **(C)** fetal lung volume measured on coronal T2-weighted fast-spin-echo sequences, and **(D)** length of the cervix from internal to external as measured on sagittal T2-weighted fast-spin-echo sequences (cervical length). The black line shows the regression analysis from respective large literature studies on normative values and the dotted lines the reported 5th and 95th quartile ranges. Squares and crosses mark the pregnant participants with a neurological finding and a placental pathology or diabetes type I, respectively. **(E, G)** Bland-Altman plots show differences (diff) in biparietal diameter and transcerebellar diameter measurements between two observers, and **(F, H)** scatterplots show the biparietal diameter and transcerebellar diameter of all cases as observed by both observers.

well in line with 1.5-T and 3-T values (Table 3). Finally, a negative correlation between brain T2* and gestational age can be observed (6.8 msec of decay per week; $R^2 = 0.54$; $P < .001$), with the data at the highest field strength again displaying the lowest overall values for the same gestational age and the data from low field strength on average with the highest values (Fig 6D). The mean placental ADC values at 0.55 T (Fig 6E, Table S3) showed, similar to higher field, more variation ($-0.068 \text{ m}^2/\text{sec}$ per week; $R^2 = 0.2$; $P < .001$) with gestational age. The perfusion fraction showed no evidence of a correlation (Fig 6F) with gestational age (0.09% decay per week; $R^2 = 0.02$; $P = .37$). The mean difference between placental T2* values for the repeated acquisitions was 10.8 msec (Fig 6G, 6H).

Finally, the specific absorption rate measurements (reported in percentage of limit) performed in participants undergoing both low- and high-field-strength imaging on the same day to assess any increase in temperature, which can be associated with the radiofrequency pulses applied during MRI examinations, were $11.4\% \pm 0.024$ for the 0.55-T examination and $93.3\% \pm 7.6$ for the 3-T examination, or in time-weighted average radiofrequency magnetic field exposure (known as B + rms; averaged over the sequence) $2.9 \mu\text{T} \pm 0.0$ at 0.55-T and $2.0 \mu\text{T} \pm 0.1$ at 3-T examinations.

Exemplar results using simultaneous multisection imaging, allowing for imaging of multiple sections within the same excitation, accelerating by a factor of two, are shown in Figure S4

and results in three pregnant participants with BMIs greater than 35 are in Figure S5.

Discussion

The use of a commercially available low-field-strength MRI system operating at 0.55 T in a sample of pregnant women using a short, clinically feasible protocol consisting of anatomic imaging and dedicated quantitative imaging without artifact-reducing techniques was able to produce high-quality, robust, and clinically useful qualitative and quantitative images in the fetus and placenta while depicting the advantages of low-field-strength imaging. All protocols and sequences used in this study can be directly shared with interested researchers, enhancing its impact and repeatability.

The reported anatomic measurements, including lung, brain parameters, and cervix, showed excellent agreement with data available from large sample studies (18–23). Repeat experiments and a low interobserver variability highlighted robustness, essential for future clinical and research applications.

Quantitative values of placenta and brain demonstrated an expected reduction in mean T2* over gestation (11), with higher absolute values (in milliseconds) given field strength. The spatial distribution of T2* within both the placenta and brain were as expected. In samples with known reduced T2* (eg, pre-eclampsia), there was a higher dynamic range in T2*.

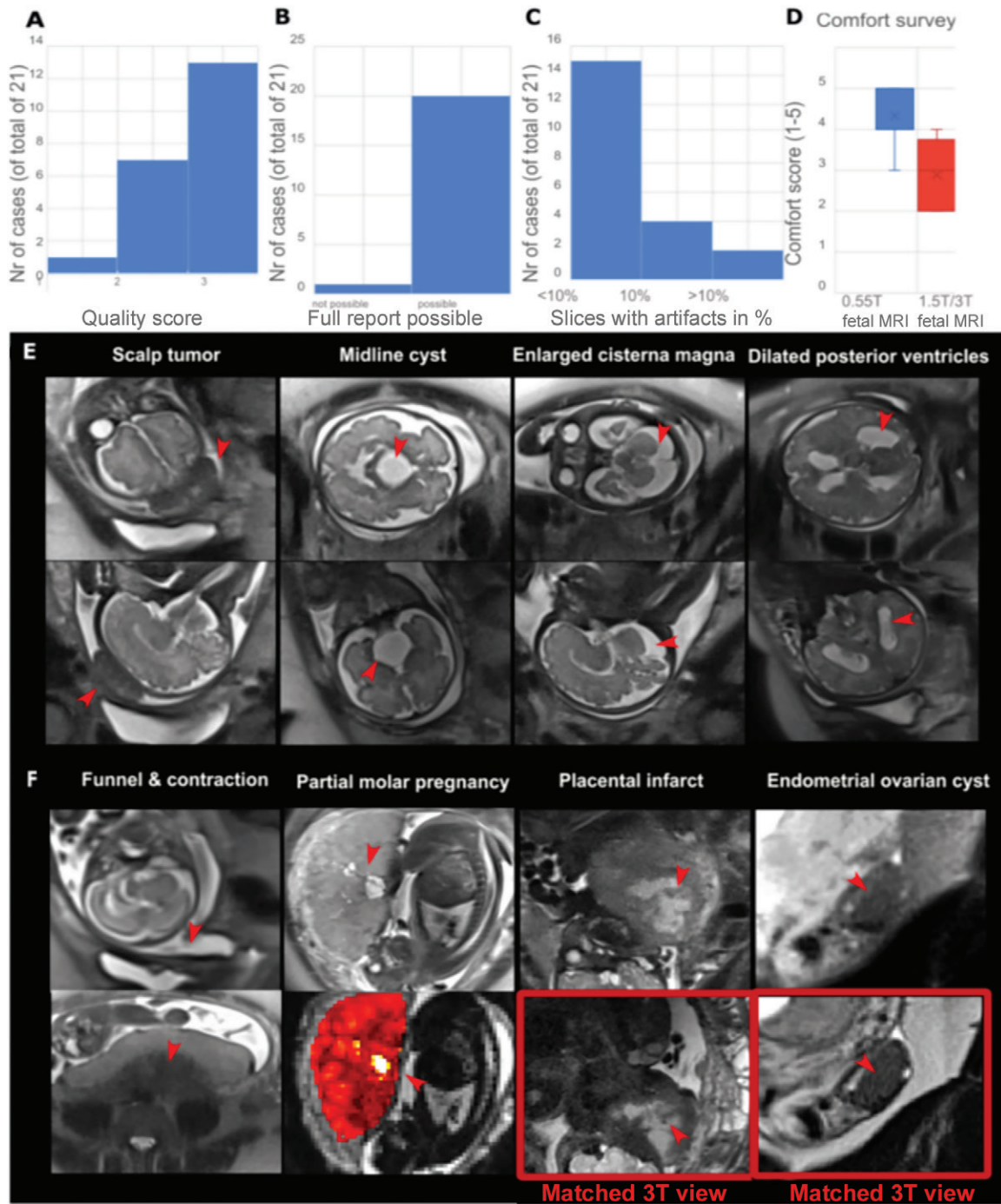


Figure 4: Quantitative assessment of the data quality and observation of relevant clinical findings and incidental findings. **(A)** Bar graph shows histograms of the clinical reporting quality for the 21 clinically referred participants with pregnancy-related pathologic abnormalities. Quality scores are defined as follows: 1, incomplete brain coverage or severe motion artifact; 2, images in all three planes covering the entire brain but rotated; and 3, all three planes, full coverage with no rotation. **(B)** “Full report possible” signifies that biparietal diameters and occipital-frontal diameter for skull and brain, transcerebellar diameter, vermis height, pons diameter, globe diameter, cavum diameter, ventricular diameters, and callosal length were assessed. **(C)** Sections (referred to as slices) with artifacts in percentages and **(D)** results from the patient comfort survey on a scale of 1–5, with 1 indicating not comfortable and 5 indicating very comfortable. **(E)** Images show (from left to right) neurologic findings (arrowheads): scalp tumor (gestational age, 34 + 0 weeks) on coronal (top) and sagittal (bottom) view, midline cyst (gestational age, 30 + 6 weeks) on axial (top) and coronal (bottom) view, enlarged cisterna magna (gestational age, 35 + 6 weeks) on axial (top) and sagittal (bottom) view, and dilated posterior ventricles (gestational age, 31 + 1 weeks) on axial (top) and coronal (bottom) view. **(F)** Images show (from left to right) funnel and uterine contraction in a participant with threatened preterm labor (gestational age, 24 + 0 weeks) on maternal sagittal (top) and axial (bottom) view and partial molar pregnancy (gestational age, 33 + 1 weeks) on coronal view (top) and functional T2* map (in color; arrowheads show an area of high T2*) coronal view (bottom); and placental infarct (gestational age, 36 + 3 weeks) and endometrial ovarian cyst (gestational age, 24 + 3 weeks) on maternal coronal views with available comparisons at higher 3-T field strength for placental artifact and endometrial ovarian cyst. Nr = number.

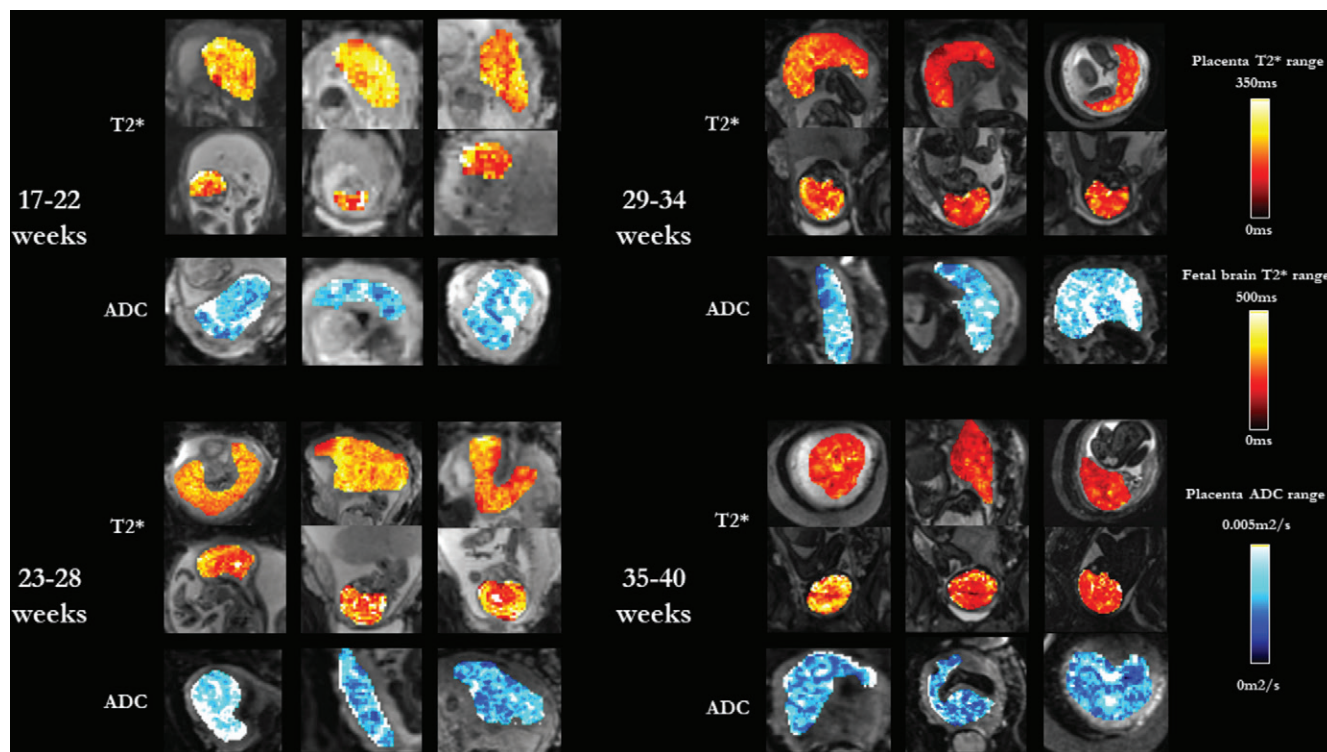


Figure 5: Images show quantitative T2* maps and apparent diffusion coefficient (ADC) maps for gestational age, split into four ranges: 17–22 weeks, 23–28 weeks, 29–34 weeks, and 35–40 weeks. T2* maps are overlaid over the data from the second echo time and the ADC maps over the data acquired at $b = 0 \text{ m}^2/\text{s}^2$. Derived quantitative maps displayed a pattern of high T2* in the lobule centers (yellow) with reduced T2* in the placental septa and toward the periphery of the placenta.

The placental diffusion values followed the previously reported decrease (5–7) but exhibited more variation. This could be linked to the conservative segmentation used here, carefully avoiding maternal tissues to focus on the placental parenchyma.

The reduction in image degradation related to magnetic field susceptibility effects and avoidance of specific shimming (21) was explored, and the possible decrease in time and need for expertise both contributed to widening access and reducing costs of fetal MRI.

Previous 0.5-T fetal imaging relied on dedicated echo-planar imaging scanners (22,24,25), whereas our study was able to leverage the latest developments in MRI sequences including simultaneous multisection imaging and advanced diffusion schemes (5,6,26,27). Perfusion MRI in the placenta as performed previously (28,29) was not included because of time restrictions.

Compared with other recently published studies regarding low-field-strength scanners (30), our study was performed by using a commercially available system, which facilitates clinical translation. Furthermore, the commercially available system offers an 80-cm bore, which clearly demonstrated improved patient experience. The MRI system we used includes a gradient system, which together with the lower field strength results in longer echo times for the echo-planar imaging sequence for similar b values, compared with conventional MRI scanners. However, the longer intrinsic T2* enabled longer readouts with similar signal strength. The resolution for the fast-spin-echo scans was reduced compared with high field strength to ensure sufficient signal-to-noise ratio. No significant increase in imaging time was observed for the considered examinations.

The reduction in helium consumption and resulting omission of a quench pipe and the low weight and short height of the system reduced the overall cost. Furthermore, the reduction in artifacts allowed the user to forego correction tools and hence reduced the need and cost for specialist operators.

Our study had limitations. First, the sample may not have represented a clinical population because opportunistic recruitment resulted in an overwhelmingly healthy study sample. Second, our study included a small number of participants. Third, for the purposes of demonstrating the ability to reproduce commonly acquired contrast and quantification techniques for fetal MRI, the widespread intravoxel incoherent motion model was used. However, different diffusion models are available, and more b values would be beneficial.

In conclusion, low-field-strength 0.55-T fetal MRI was capable of producing reliable structural and functional measures of the fetus and placenta in pregnancy using a commercially available 0.55-T MRI scanner and a comprehensive 20-minute protocol. Our protocol offered multiple advantages in an easy-to-acquire 20-minute fetal MRI examination: it reduced the occurrence of artifacts and therefore the need for time-consuming corrections; it provided longer sampling along echo trains; and it provided higher quality T2* data, thus increasing patient accessibility. Therefore, these results offer the potential for increased patient accessibility because of shorter time requirements and a larger bore and allowed for wider use by reducing costs and removing the need for specialist techniques. Future work should include a dedicated high-risk study sample and additional fetal body anomalies. In samples with known reduced T2* (eg, pre-eclampsia), the higher dynamic range

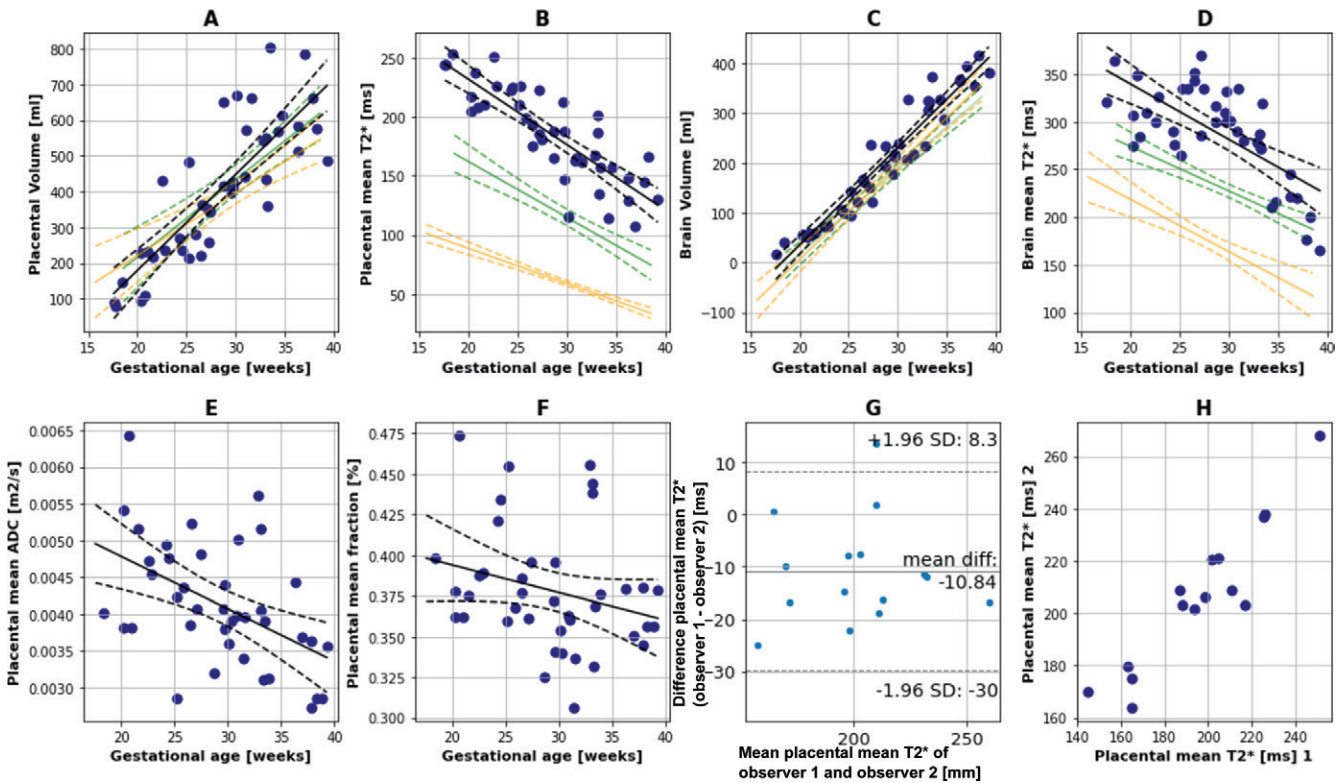


Figure 6: Plots show quantitative volume T2* and apparent diffusion coefficient (ADC) results at different gestational ages in healthy pregnant participants. (A) Placental volume from T2* scan in milliliters, (B) placental mean T2* in milliseconds, (C) fetal brain volume in milliliters from T2* scan, and (D) mean fetal brain T2* in milliseconds. Measurements from the 0.55-T low-field-strength MRI study (blue dots) and regression results from 1.5 T (green lines) and 3 T (orange lines) are shown. The results from both diffusion models in the placenta are shown in (E) mean placental ADC and (F) mean perfusion fraction. (G) Bland-Altman plot shows differences in measurements for the repeated T2* scans. diff = difference. (H) Scatterplot shows T2* results from repeat scans.

in T2* warrants further exploration, potentially allowing for finer determination of the pathologic processes, including architectural placental processes resulting in a mature villous tree. More paired participants who undergo both low- and high-field-strength examinations on the same day would provide further evidence of the potential advantages of low-field-strength scanning. Analyzing myelination in future studies could further examine the positive effects of shorter T1 in reducing artifacts, which could yield further advantage by improving contrast enhancement. In addition, future work could focus on possible tissue contrast enhancement, perfusion techniques, and noncontrast-enhanced angiography, and may explore techniques and sequences exploiting the longer T2* and ability for longer readouts.

Acknowledgments: The authors thank all of the pregnant women and their families for taking part in this study. The authors thank Imogen Desforges, BSc, Chidinma Iheanetu Oguejiofor, MSc, and Maggie Lee for their invaluable efforts in recruiting and looking after the women in this study as well as Kathleen Colford, BSc, Massimo Marenzana, PhD, Philippa Bridgen, BSc, and Peter Murkin, MA, for their involvement in the acquisition of these data sets.

Author contributions: Guarantors of integrity of entire study, J.V.H., J.H.; study concepts/study design or data acquisition or data analysis/interpretation, all authors; manuscript drafting or manuscript revision for important intellectual content, all authors; approval of final version of submitted manuscript, all authors; agrees to ensure any questions related to the work are appropriately resolved, all authors; literature research, J.A.V., M.A.R., R.T.T., J.H.; clinical studies, J.A.V., L.S., M.H., A.E., M.A.R., R.T.T., J.H.; experimental studies, J.A.V., J.V.H., R.T.T., J.H.; statistical analysis, J.A.V., P.T.S.; and manuscript editing, J.A.V., L.S., M.H., T.F., P.T.S., S.J.M., M.A.R., J.V.H., R.T.T., J.H.

Data sharing: Data generated or analyzed during the study are available from the corresponding author by request.

Disclosures of conflicts of interest: J.A.V. Support from EPSRC Doctoral Training Partnership. L.S. Grants from the Leona M and Harry B Helmsley Charitable Trust; MRC Medical Research Council; BMFMS British Maternal and Fetal Medicine Society; KHP Research and Development challenge fund; NIHR National Institute For Health and Care Research; J P Moulton Charitable Foundation; Academy of Medical Sciences. Scientific editor, *British Journal of Obstetrics and Gynecology*. Participant on a scientific advisory board, Royal College of Obstetricians Gynecologists. M.H. No relevant relationships. T.F. No relevant relationships. A.E. No relevant relationships. P.T.S. No relevant relationships. S.J.M. No relevant relationships. M.A.R. No relevant relationships. J.V.H. Funded by Siemens; grant from Wellcome Trust; equipment loan from Siemens Healthineers. R.T.T. Employee, Siemens Healthcare. J.H. Grant support, Wellcome Trust; MRC funding; EPSRC funding. Advisory board membership, Wellcome Open Research.

References

- Hart AR, Embleton ND, Bradburn M, et al. Accuracy of in-utero MRI to detect fetal brain abnormalities and prognosticate developmental outcome: postnatal follow-up of the MERIDIAN cohort. *Lancet Child Adolesc Health* 2020;4(2):131–140.
- Lloyd DFA, Pushparajah K, Simpson JM, et al. Three-dimensional visualisation of the fetal heart using prenatal MRI with motion-corrected slice-volume registration: a prospective, single-centre cohort study. *Lancet* 2019;393(10181):1619–1627.
- Story L, Zhang T, Steinweg JK, et al. Foetal lung volumes in pregnant women who deliver very preterm: a pilot study. *Pediatr Res* 2020;87(6):1066–1071.
- Story L, Davidson A, Patkee P, et al. Brain volumetry in fetuses that deliver very preterm: An MRI pilot study. *Neuroimage Clin* 2021;30:102650.
- Jakab A, Tuura RL, Kottke R, et al. Microvascular perfusion of the placenta, developing fetal liver, and lungs assessed with intravoxel incoherent motion imaging. *J Magn Reson Imaging* 2018;48(1):214–225.

6. Antonelli A, Capuani S, Ercolani G, et al. Human placental microperfusion and microstructural assessment by intra-voxel incoherent motion MRI for discriminating intrauterine growth restriction: a pilot study. *J Matern Fetal Neonatal Med* 2022;35(25):9667–9674.
7. Hutter J, Slator PJ, Jackson L, et al. Multi-modal functional MRI to explore placental function over gestation. *Magn Reson Med* 2019;81(2):1191–1204.
8. Slator PJ, Palombo M, Miller KL, et al. Combined diffusion-relaxometry microstructure imaging: Current status and future prospects. *Magn Reson Med* 2021;86(6):2987–3011.
9. Arthurs OJ, Rega A, Guimiot F, et al. Diffusion-weighted magnetic resonance imaging of the fetal brain in intrauterine growth restriction. *Ultrasound Obstet Gynecol* 2017;50(1):79–87.
10. Schabel MC, Roberts VHJ, Lo JO, et al. Functional imaging of the nonhuman primate Placenta with endogenous blood oxygen level-dependent contrast. *Magn Reson Med* 2016;76(5):1551–1562.
11. Sørensen A, Hutter J, Seed M, Grant PE, Gowland P. T2*-weighted placental MRI: basic research tool or emerging clinical test for placental dysfunction? *Ultrasound Obstet Gynecol* 2020;55(3):293–302.
12. Sinding M, Peters DA, Frøkjær JB, et al. Placental magnetic resonance imaging T2* measurements in normal pregnancies and in those complicated by fetal growth restriction. *Ultrasound Obstet Gynecol* 2016;47(6):748–754.
13. Ho AEP, Hutter J, Jackson LH, et al. T2* Placental Magnetic Resonance Imaging in Preterm Preeclampsia: An Observational Cohort Study. *Hypertension* 2020;75(6):1523–1531.
14. Steinweg JK, Hui GTY, Pietsch M, et al. T2* placental MRI in pregnancies complicated with fetal congenital heart disease. *Placenta* 2021;108:23–31.
15. Merkle EM, Dale BM, Paulson EK. Abdominal MR imaging at 3T. *Magn Reson Imaging Clin N Am* 2006;14(1):17–26.
16. Creanga AA, Catalano PM, Bateman BT. Obesity in Pregnancy. *N Engl J Med* 2022;387(3):248–259.
17. Kyriakopoulou V, Vatansver D, Davidson A, et al. Normative biometry of the fetal brain using magnetic resonance imaging. *Brain Struct Funct* 2017;222(5):2295–2307.
18. Masselli G, Perrone G, Kinkel K, et al. Are Second Trimester Apparent Diffusion Coefficient Values of the Short Uterine Cervix Associated with Impending Preterm Delivery? *Radiology* 2016;280(3):897–904.
19. Snijders RJ, Nicolaides KH. Fetal biometry at 14–40 weeks' gestation. *Ultrasound Obstet Gynecol* 1994;4(1):34–48.
20. Chavez MR, Ananth CV, Smulian JC, Lashley S, Kontopoulos EV, Vintzileos AM. Fetal transcerebellar diameter nomogram in singleton gestations with special emphasis in the third trimester: a comparison with previously published nomograms. *Am J Obstet Gynecol* 2003;189(4):1021–1025.
21. Gaspar AS, Nunes RG, Ferrazzi G, et al. Optimizing maternal fat suppression with constrained image-based shimming in fetal MR. *Magn Reson Med* 2019;81(1):477–485.
22. Gowland P, Fulford J. Initial experiences of performing fetal fMRI. *Exp Neurol* 2004;190(Suppl 1):S22–S27.
23. Rypens F, Metens T, Rocourt N, et al. Fetal lung volume: estimation at MR imaging—initial results. *Radiology* 2001;219(1):236–241.
24. Gowland P. Placental MRI. *Semin Fetal Neonatal Med* 2005;10(5):485–490.
25. Gowland PA, Freeman A, Issa B, et al. In vivo relaxation time measurements in the human placenta using echo planar imaging at 0.5 T. *Magn Reson Imaging* 1998;16(3):241–247.
26. Andescavage N, Kapse K, Lu YC, et al. Normative placental structure in pregnancy using quantitative Magnetic Resonance Imaging. *Placenta* 2021;112:172–179.
27. Slator PJ, Hutter J, Marinescu RV, et al. InSpect: INtegrated SPECTral Component Estimation and Mapping for Multi-contrast Microstructural MRI. In: Chung A, Gee J, Yushkevich P, Bao S, eds. *Information Processing in Medical Imaging. IPMI 2019. Lecture Notes in Computer Science*, vol 11492. Springer, 2019; 755–766.
28. Hutter J, Harteveld AA, Jackson LH, et al. Perfusion and apparent oxygenation in the human placenta (PERFOX). *Magn Reson Med* 2020;83(2):549–560.
29. Zun Z, Zaharchuk G, Andescavage NN, Donofrio MT, Limperopoulos C. Non-Invasive Placental Perfusion Imaging in Pregnancies Complicated by Fetal Heart Disease Using Velocity-Selective Arterial Spin Labeled MRI. *Sci Rep* 2017;7(1):16126.
30. Restivo MC, Ramasawmy R, Bandettini WP, Herzka DA, Campbell-Washburn AE. Efficient spiral in-out and EPI balanced steady-state free precession cine imaging using a high-performance 0.5T MRI. *Magn Reson Med* 2020;84(5):2364–2375.